Biomedicine & Pharmacotherapy 109 (2019) 1052–1061

Contents lists available at ScienceDirect

Biomedicine & Pharmacotherapy

journal homepage: www.elsevier.com/locate/biopha

Protective and reversal actions of a novel peptidomimetic against a pivotal toxin implicated in Alzheimer's disease

Giovanni Ferrati[a,*], Georgi Bion[a], Andrew J. Harris[b], Susan Greenfield[a]

[a] Neuro-Bio Ltd, Culham Science Centre, Building F5, Abingdon, OX14 3DB, UK
[b] Pharmidex, European Knowledge Centre, Hatfield, Hertfordshire, AL10 9SN, UK

ARTICLE INFO

Keywords:
Acetylcholinesterase
Alzheimer's disease
α7 nicotinic receptor
Peptidomimetic
Voltage-sensitive dye imaging
Ex vivo

ABSTRACT

Despite the many attempts to understand the aetiology of Alzheimer's disease, the basic mechanisms accounting for the progressive cycle of neuronal loss are still unknown. Previous work has suggested that the pivotal molecule mediating neurodegeneration could be an independently acting peptide cleaved from acetylcholinesterase. This previously unidentified agent acts as a signalling molecule in selectively vulnerable groups of cells where erstwhile developmental mechanisms are activated inappropriately to have a toxic effect in the context of the mature brain. We have previously shown that the toxic actions of this peptide, whose level is doubled in the Alzheimer brain, can be blocked by a cyclised variant (NBP14). However, the size and properties of NBP14 would render it unlikely as a feasible therapeutic candidate. Here therefore we test a synthetic peptidomimetic (NB-0193), modelled on the binding of NBP14 to the target alpha-7 nicotinic receptor, and benchmarked against it to screen for reversal effects using real-time optical imaging in rat brain slices. The blocking action of NB-0193 was confirmed by testing its effect against peptide-induced calcium influx in cell cultures, where it showed a dose-dependent profile over a trophic-toxic range. Moreover, NB-0193 presented promising pharmacokinetic characteristics and could therefore prompt a new therapeutic approach against Alzheimer's disease.

1. Introduction

Neurodegenerative disorders are defined as hereditary and sporadic conditions characterized by progressive nervous system dysfunction [1,2]. Dementias are the most severe symptom of neurodegenerative diseases, of which Alzheimer's disease (AD) is the most common, representing approximately 60–70% of the total [1]. Although there have been many attempts to explain the possible causes for Alzheimer's disease, the basic mechanism remains unidentified, that drives the continued neuronal loss underlying the progression of the disease. Interestingly, an interconnecting core of adjacent subcortical groups of cells distributed throughout basal forebrain-midbrain-brainstem are particularly vulnerable to neurodegenerative events [3–8]. These cells, collectively termed 'global neurons' [9,10] form a continuous hub and, despite a heterogeneity of transmitters, are characterised by key common features: in particular, these diverse cell groups all contain the enzyme acetylcholinesterase (AChE) regardless of, in most cases (e.g. substantia nigra, raphe nuclei, locus coeruleus), the absence of its conventional substrate, acetylcholine. Although well known as an enzyme, AChE can also have a non-classical function [4,11–14] mediated by a peptide cleaved from its C-terminus (AChE-peptide) [11] (Fig. 1 i). More specifically, this peptide of 30 residues (T30), composed of a bioactive 14 amino-acid sequence (T14) followed by an inert portion at the C-terminal (T15) [15–17] (Fig. 1 ii), has been implicated in enhancing calcium entry in the cells through an allosteric site at the α7 nicotinic receptor (α7-nAChR) [18], mediating trophic or toxic actions according to dose, duration of exposure [20] and neuronal age [5,21]. During aging, the aberrant reactivation of trophic pathways in specific conditions (i.e. stroke, injuries, decline in free radical scavenging mechanisms etc.) can induce compensating responses in global neurons in an attempt to regenerate subsequently bringing to calcium influx dysregulation, particularly dangerous in mature cells: hence neurodegeneration could be an inappropriate form of development [1,5]. AChE-peptide bioactivity has already been demonstrated in different preparations resulting in trophic-toxic effects in organotypic cell cultures and neuronal cell lines [17–19,22], upregulation of α7-nAChRs [15], and enhancement of calcium potentials in mammalian brain slices [23].

Here, for the first time the previously established effect of T30 was assessed at five different dilutions (1, 2, 5, 10 and 20 μM) on voltage sensitive dye imaging (VSDI) - a technique that enables the study of

* Corresponding author.
E-mail address: giovanni.ferrati@neuro-bio.com (G. Ferrati).

https://doi.org/10.1016/j.biopha.2018.10.124
Received 5 July 2018; Received in revised form 19 October 2018; Accepted 21 October 2018

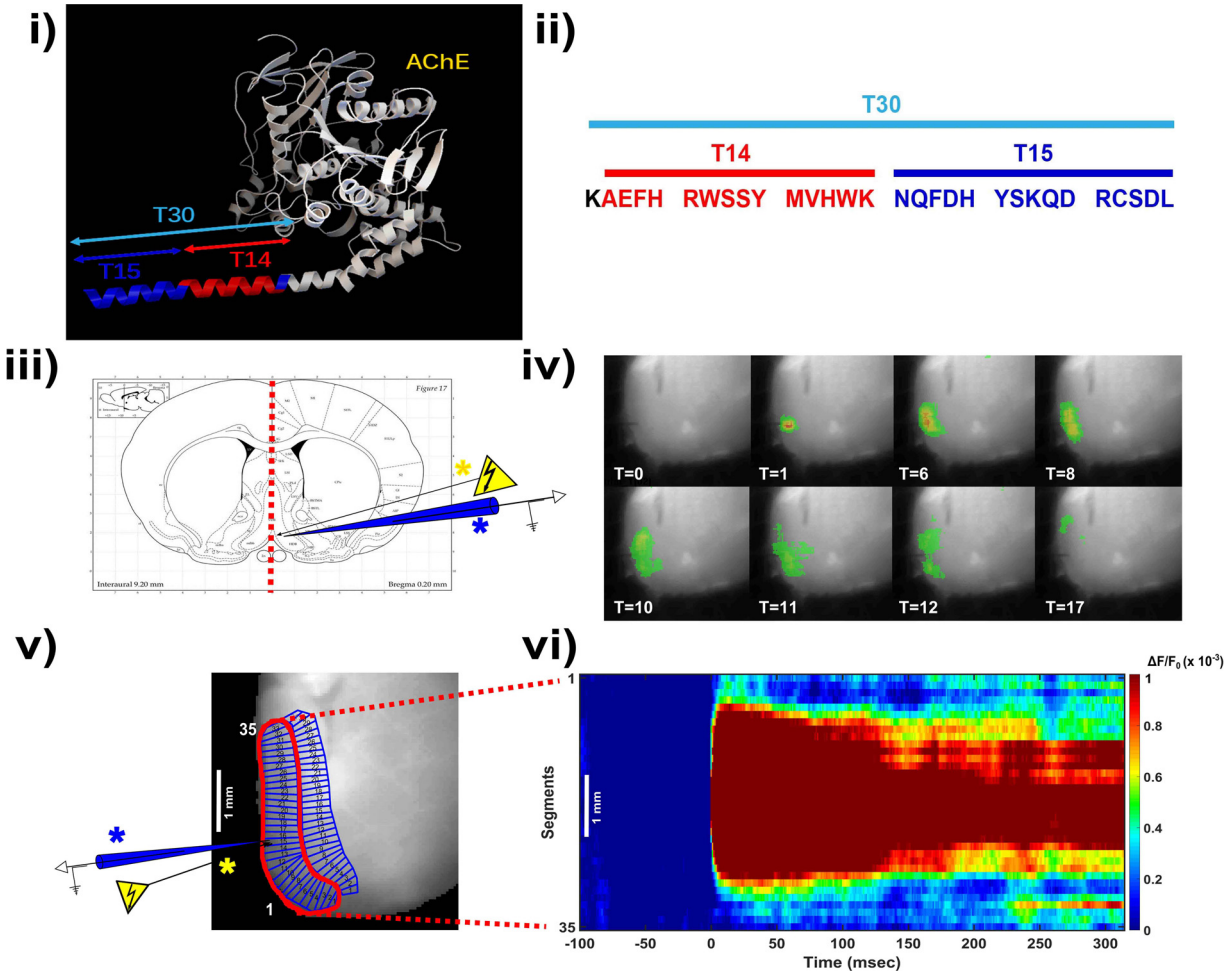

Fig. 1. T30 sequence and response analysis from BF-containing slices. Ribbon model of AChE structure (i) with the C-terminus coloured to highlight the T30 inert part (T15, blue) and its bioactive portion T14 (red). (ii) Amino acidic sequence of T30, from which the cyclised (NBP14) and linear (NB-0193) variant blockers are synthesised. Coronal section (iii) from the rat brain atlas [42] indicating the area where the stimulating electrode (yellow asterisk) and the recording electrode (blue asterisk) are placed. Raw data indicating the meso-scale neuronal response at different time points after stimulation of the basal forebrain (iv) from a P14 animal. ROI selection (in red) and segmentation (v) used to categorise VSDI data into arrays of activity over time. Representative 'space-time' map (vi, P14 rats, n = 10) of BF population response to electric stimulation (v, yellow asterisk).

meso-scale brain activity in real-time [24–26] - in rat brain slices containing the basal forebrain (BF), suggested to be one of the primary affected areas in AD [27,28]. Previous studies have demonstrated an effect of a cyclised variant, NBP14, of the active 14mer in both protecting against its toxicity in PC12 cells [17] as well as actually reversing the action of the peptide in rat brain slices [29]. We used NBP14 as a benchmark to evaluate a peptidomimetic, NB-0193, that would have more promising therapeutic potential in view of its smaller size both protecting against, and even reversing, the T30 toxicity.

2. Materials and methods

2.1. Animals

Male Wistar rats (Charles River, United Kingdom) of age postnatal day 14 (P14) were used for optical imaging experiments while male Nude Balb/c mice (Harlan, United Kingdom) were used for pharmacokinetics assays. All animal procedures are approved by the Home Office UK (according to "Schedule 1″ regulations) and conducted in compliance with the requirements of the UK Animals (Scientific Procedures) Act 1986.

2.2. Brain slice preparation

Preparation of the sections was carried out as previously described [29]. In summary, three consecutive 400 µm thick rat brain slices containing the basal forebrain (1.20 to 0.00 mm from Bregma) were sectioned using a Leica VT1000S vibratome. The sections comprised different areas including: the medial septum (MS), the vertical diagonal band (VDB) and the horizontal diagonal band (HDB), the substantia innominata (SI) including the nucleus basalis of Meynert (NBM). Consecutively, each slice was cut along the midline in two hemisections which were transferred to a bubbler pot with artificial cerebro-spinal fluid (aCSF) ('recording' aCSF in mmol: 124 NaCl, 3.7 KCl, 26 $NaHCO_3$, 2 $CaCl_2$, 1.3 $MgSO_4$, 1.3 KH_2PO_4 and 10 glucose; pH: 7.1) and incubated at 34 °C for 20 min (min). The hemisections were kept at room temperature (RT) for 30 min in oxygenated (95% O_2, 5% CO_2) aCSF to recuperate before VSD staining.

2.3. Optical and electrophysiology field recording method

Each electrophysiology and VSDI experiment was performed as formerly described [29]. Briefly, excitatory postsynaptic potential (fEPSP) recordings and optical imaging using a voltage-sensitive dye, Di-4-ANEPPS (4% 0.2 mM styryl dye pyridinium 4-[2-[6-(dibutylamino)-2-aphthalenyl]-ethenyl]-1-(3-sulfopropyl)hydroxide; Sigma-

Aldrich, D8064, Germany), dissolved in aCSF (artificial cerebro-spinal fluid), fetal bovine serum 48%, DMSO 3.5% and cremophore EL 0.4%), were subsequently carried out after a 20 min incubation with the dye. Sections were then transferred and kept in aCSF (at room temperature, 22 °C ± 1.5 °C) for 45 min to wash off the dye excess and favour the recovery phase. The dye was chosen because it is characterised by minimal pharmacological side effects or phototoxicity and a high signal-to-noise ratio [30].

After incubation with the dye, for each imaging session, hemisections were placed in the recording bath, continuously perfused with oxygenated aCSF (in mmol: 124 NaCl, 3.7 KCl, 26 $NaHCO_3$, 2 $CaCl_2$, 1.3 $MgSO_4$, 1.3 KH_2PO_4 and 10 glucose; pH: 7.1) and warmed to 30 °C ± 1 °C with a temperature control system (TC-202 A, Digitimer Research Instruments, Hertfordshire, UK). Slices were kept in position with a home-made plastic grid before placing the stimulating electrode (Pt-Ir concentric bipolar FHC electrodes, Bowdoin, USA; outer pole diameter 200 μm, inner pole diameter 25 μm) and the recording electrode in an area of the BF comprised between the HDB and VDB (Fig. 1 iii, iv, v). Each experimental session consisted of a 25 min perfusion epoch per different treatment, subdivided in a 15 min recording period preceded by a 10 min slice acclimatisation to the recording bath.

2.4. Data analysis

Each experiment electrophysiology and VSDI experiment was analysed as previously described [29]. In short, optical imaging data were processed using a toolbox implemented in MatLab (The Mathworks Inc, USA) [31]. The region of interest was post-hoc visually drawn onto the slice to comprehend the global evoked VSDI responses of the BF area (Fig. 1 v). VSDI data refer to results from the selected ROI plotted as the magnitude of BF activity over space and time ('space-time' maps, Fig. 1 vi), as summed fluorescence fractional change indicated by the value calculated from the area under the curve between 0 and 300 ms (ms) after stimulation delivery ($\Sigma\Delta F/F_0$), or as averaged summed activity. The colour map employs warm and cool colours representing depolarization or no response.

2.5. PC12 cell culture and calcium influx assay

Cell culture and calcium influx assays were performed as previously described [17]. Briefly, wild-type PC12 cells (Sigma-Aldrich, St. Louis, MO) were routinely plated in collagen-coated (2 mg/cm^2) 100 mm dishes (Corning) and maintained in growth medium with Eagle's minimum essential medium (MEM) supplemented with heat-inactivated 10% horse serum (HS) and 5% foetal bovine serum (FBS), 10 mM 4-(2-hydroxyethyl)- 1-piperazineethanesulfonic acid (HEPES), 2 mM L-Glutamine and 1:400 Penicillin/streptomycin solution. Cultures were maintained at 37 °C in a humidified incubator with 5% CO_2/95% air and the medium was replaced every 2 days.

For calcium fluorimetry, cells were plated in 200 ml of DMEM (Dulbecco's Modified Eagle's medium) plus 2 mM of L-glutamine medium the day before the experiment in 96 well plates. On the day of the experiment, the Fluo-8 solution (Abcam, UK) was prepared as described by the manufacturer. After removal of 100 ml of growth medium, an equal amount of Fluo-8 solution was added. T30 and/or NB-0193 were added and left for 30 min in the incubator and 30 min at room temperature. One hour after, the plate was placed in the fluorescence plate reader (Fluostar, Optima, BMG Labtech, Ortenberg, Germany). Before reading the fluorescence, acetylcholine (ACh) 100 μM, an agonist of the nicotinic receptors, was prepared and placed in the Fluostar injector. The basal fluorescence was calculated first, followed by acetylcholine injection which induces calcium increase via nicotinic receptors.

2.6. In silico peptidomimetic identification

The procedure followed for the peptidomimetic design was subdivided in three steps:

Phase I: Solvent mapping. The computation solvent mapping was conducted over the starting initial X-ray structure. This analysis was aimed to elucidate the preferential solvent interaction at the binding site as well as to locate the presence of hot spots (hydrophobic, aromatic, polar or charged). This method identifies the expected chemical features required by the ligand in order to become active.

The IPRO solvent analysis unravelled the high hydrophobic nature of the binding site. Perfect overlapping between IPRO solvent mapping prediction and T14 peptide docking was observed. For T14, docking was conducted with AutoDock Vina 1.1.2 and exhaustiveness was set up to 100 and an energy window of 10 kcal/mol was allowed to be sampled by an initial extended linear T14 peptide conformation, rendering an affinity of -8.1 kcal/mol.

Phase II: Library generation. The pentameric α-7-nicotinic receptor (PDB code: 3SQ6) was subjected to the computational IPRO Technology workflow. Based on the solvent mapping analysis, the T14 structure was used for the generation of multiple cyclic libraries. More than 1,5 M cyclic peptidomimetics were generated with the IPRO Technology. These peptidomimetics were encompassed into 174 peptide scaffolds, differentiated by the intramolecular amide bond formed between the side-chains in order to obtain the cyclic geometry. In addition to the cyclic libraries, linear libraries of tripeptides and tetrapeptides were generated. In this case, more than 500 K peptidomimetics were generated for a further evaluation.

In total, more than 2 M of peptidomimetics were specifically generated. All libraries were enriched with hydrophobic amino acids accordingly to the IPRO solvent prediction.

Phase III: Final evaluation. In total, more than 1,5 M cyclic and lineal peptides and 500 K linear peptides have been evaluated by AutoDock Vina docking engine. The theoretical affinities as well as ligand promiscuity (i.e, tendency to bind in multiple binding sites or different binding modes, denoted by a low intra-RMSD) were taken into account for the analysis. Only those peptide structures retaining a high affinity and low intra-RMSD were selected. After analysis and in silico clustering, a list of 20 non-redundant peptides whose structure is compatible each other (in order to derive Structure-Activity Relationships after experimental evaluation) was generated and the final compound chosen based on a compromise between a high affinity and low molecular weight.

2.7. Permeability assay

Experiments were performed by Pharmidex (London, United Kingdom). All compounds were dissolved in suitable solvent to provide 10 mM stock solutions from which donor (dose) solutions were prepared in DMEM to give a final drug concentration of 10 μM. Bidirectional permeability measurements were derived by examining the transfer of the compound in both the apical to basolateral compartment across a cell monolayer, and vice versa over a 90- minute period. The assay used was a MDCK-MDR1 (Madin-Darby canine kidney cells transfected with the human MDR1 gene - multi-drug resistance gene 1 - as a model of the human intestinal mucosa) directional permeability assay at 10 μM concentration of both drugs (NBP14 and NB-0193) with control compounds (10 μM propranolol used as an internal standard for passive permeability and labetolol for P-gp, or permeability Glycoprotein, assessment). Efflux ratio was calculated from the mean apical to basolateral (A–B) apparent permeability coefficient (Papp) data and basolateral to apical (B-A) Papp data. Sample analysis was conducted using HPLC-MS/MS (High Performance Liquid Chromatography - triple quadrupole mass spectrometry) with the detection settings optimised for each test compound.

2.8. In vivo pharmacokinetic assessment

Experiments were performed by Pharmidex (London, United Kingdom). Three Nude Balb/c mice (Harlan, United Kingdom) were singly housed in the animal facility at the Northwick Park Institute for Medical Research and maintained under a 12 h light/dark cycle with free access to food and water, where temperature and humidity were controlled according to Home Office regulations. NBP14 and NB-0193 were then intravenously administered (n = 3 for each compound) as a bolus at 10 mg/kg with terminal sampling at 0.02, 0.05, 0.08 and 0.33 h after dosing. Immediately after collection blood samples were precipitated with 3 volumes of an ice-cold solution of internal standard prepared in Acetonitrile (MeCN). After centrifugation the supernatant samples were snap-frozen in liquid nitrogen and stored at −70 °C. Brain samples were hemi-sected, weighed, snap-frozen in liquid nitrogen and stored at −70 °C. Samples were then transferred on dry ice to the Pharmidex bioanalytical laboratory at Stevenage Bioscience Catalyst (SBC) for determination of drug concentrations. Samples were stored at SBC at −80 °C. On the day of analysis samples were thawed on ice and analysed using a specific HPLC - MS/MS method with electrospray ionisation.

2.9. Statistical analysis

Unless otherwise noted, all statistical analyses were performed using GraphPad Prism 6 (v6.05; GraphPad Software Inc., CA, USA) and, as all the data were tested for normality, only parametric tests (unpaired t tests, one-way Analysis of Variance (ANOVA) followed by Fisher LSD *post hoc* tests or by Tukey's *post hoc* test when groups number was > 3) were used. For all statistical tests, $p < 0.05$ was considered significant; data are expressed as mean ± SEM (standard error of the mean). Statistical significance: *$p < 0.05$; **$p < 0.01$, ***$p < 0.001$, ns = non-significant.

3. Results

3.1. Dose-dependent effects of AChE-peptide

Electrical stimulations of the BF elicited a significant response of neuronal population measured both with VSDI and also electrophysiology (field excitatory post-synaptic potential recordings, fEPSP) to confirm optical imaging data as a real physiological result and verify slice viability throughout long-lasting experiments [32]. A large artefact lasting about 2 ms right after stimulation was detected with fEPSP, whereas the amplitude peak was reached 5 ms after the onset. Both VSDI and electrophysiology had their maximum at approximately 5 ms after stimulus delivery, with VSDI rise being slightly slower, indicating a correlated activity and corroborating the lack of artefactual signals (Supplementary Fig. S1). The decline in assembly size - or coalitions of neurons cooperating to perform a specific computation on a sub-second scale [33] - seen with T30 can be observed in VSDI recordings both in space, being the activated area smaller in comparison with control recordings, and in time, with a weaker and shorter response to stimulation (Fig. 2 Aii). However, electrophysiological recordings do not reveal any difference amongst conditions. This discrepancy, as already demonstrated, could be because VSDI reveals small variations in membrane potential - including sub-threshold events - over a wide receptive field, whilst electrophysiology doesn't have the appropriate sensitivity to detect these changes [29].

The area under the curves (Fig. 2 i) represents the averaged summed activity. Histograms show normalised values for recordings made in control conditions and after T30 perfusion in the aCSF (Fig. 2 Aiii). T30 epochs are characterised by a 25% magnitude reduction that remains almost constant throughout the whole duration of the experiment (Fig. 2 Aiii, $F_{(1.952,\ 21.47)} = 3.476$, $p < 0.05$, n = 12, *post hoc* comparisons: see figure). To confirm that the decrease was not due to a diminished viability of the sections, we performed control experiments throughout 3 periods (Fig. 2 B). The three recordings stages with normal aCSF displayed a comparable activation (Fig. 2 Bii), with a physiological lower magnitude during the third epoch and a slightly higher response in the second one, probably due to acclimatisation of the slice to the new environment. However, no significant difference is seen in the summed fluorescence (Fig. 2 Biii, $F_{(1.762,\ 40.52)} = 0.6675$, $p = 0.50$, n = 24), substantiating the stability of the recording conditions over time.

After confirming that 2 μM T30 works as an inhibiting molecule in this preparation, we assessed increasing doses of the same molecule starting from 1 μM until 20 μM. A low concentration (1 μM, n = 17) determined a different outcome compared to baseline conditions with a marginally higher activity (Fig. 3 A) that resembles the increasing tendency detected during the second control recording epoch (see Fig. 2 Biii). Rising the T30 quantity to 5 μM (n = 11) resulted in an inhibitory profile analogous to that seen following the 2 μM dose. Specifically, after the first drug perfusion period (Fig. 3 B), response magnitude was significantly reduced in comparison with control conditions ($F_{(1.865,\ 20.52)} = 4.922$ $p < 0.05$, n = 11, *post hoc* comparisons: see figure). Interestingly higher doses i.e., 10 (n = 12) or 20 μM (n = 5) administration caused a reversal to baseline in BF neuronal activity in both cases (Fig. 3 B). In contrast, at all dilutions, the second T30 recording period displayed an overall trend towards an activity decrement against the baseline. The dose-dependent pattern observed allowed us to select the most appropriate dose of T30 for testing the benchmark NBP14 and the peptidomimetic modelled on its receptor interaction.

3.2. Blockade of T30 effects with a cyclised peptide (NBP14)

The first compound used here - already shown to counteract T30 toxicity - was NBP14 [29], a cyclised version of the 14-mer bioactive part included in the T30 (Fig. 1 ii). Nonetheless we first investigated any long-term impact on BF-containing brain sections alone in the aCSF (Fig. 4 Ai,ii,iii). No difference in response was identified compared to controls ($F_{(1.975,\ 25.67)} = 0.6521$, $p = 0.52$), confirming previous data indicating that this compound acts as an inert allosteric modulator [29]. Recently we showed a reversal of T30 action using 4 μM NBP14. In this study we extended our findings trying to determine the minimal concentration needed to exert a positive action on neuronal activity using a 1:1 ratio with the drug or double the dose. Interestingly, although a recovering trend is visible in the graph (Fig. 4 Biii) no significant effect was observed with an equal quantity ($F_{(2,\ 60)} = 0.6219$, $p = 0.54$, n = 21). Raising to 4 μM the amount of compound in the aCSF evoked a significant and strong recuperation against the toxicity attributable to T30 (Fig. 4 Ciii, $F_{(1.679,\ 25.19)} = 4.339$, $p < 0.05$, *post hoc* comparisons: see figure). The space-time maps highlight some differences between the activation profiles observed using different concentrations: while with 2 μM the recovery is characterised by a higher activity over time but not over space (Fig. 4 Bii), being the BF-activated areas quite similar in size, with 4 μM the increase in response magnitude is reflected both over time and space, as evidenced by a longer-lasting and more spatially spread neuronal assemblies (Fig. 4 Cii). A summary of the summed total averaged fluorescence over time is shown in the activation curves (Fig. 4 Bi, Ci) displaying a significant overall reduction with T30 and a recovery over time when NBP14 is co-administered with the peptide.

3.3. Design of a molecule based on NBP14: NB-0193

After confirming NBP14 as a benchmark drug successfully used in *ex vivo* as well as molecular studies [17,29], we designated the drug NB-0193 (Supplementary Fig. S2) as a new potential therapeutic based on its prototype NBP14. We aimed to identify a list of peptidomimetics - or protein-like chains - and subsequently select the new drug from this collection according to NBP14 sequence modified to adjust molecular

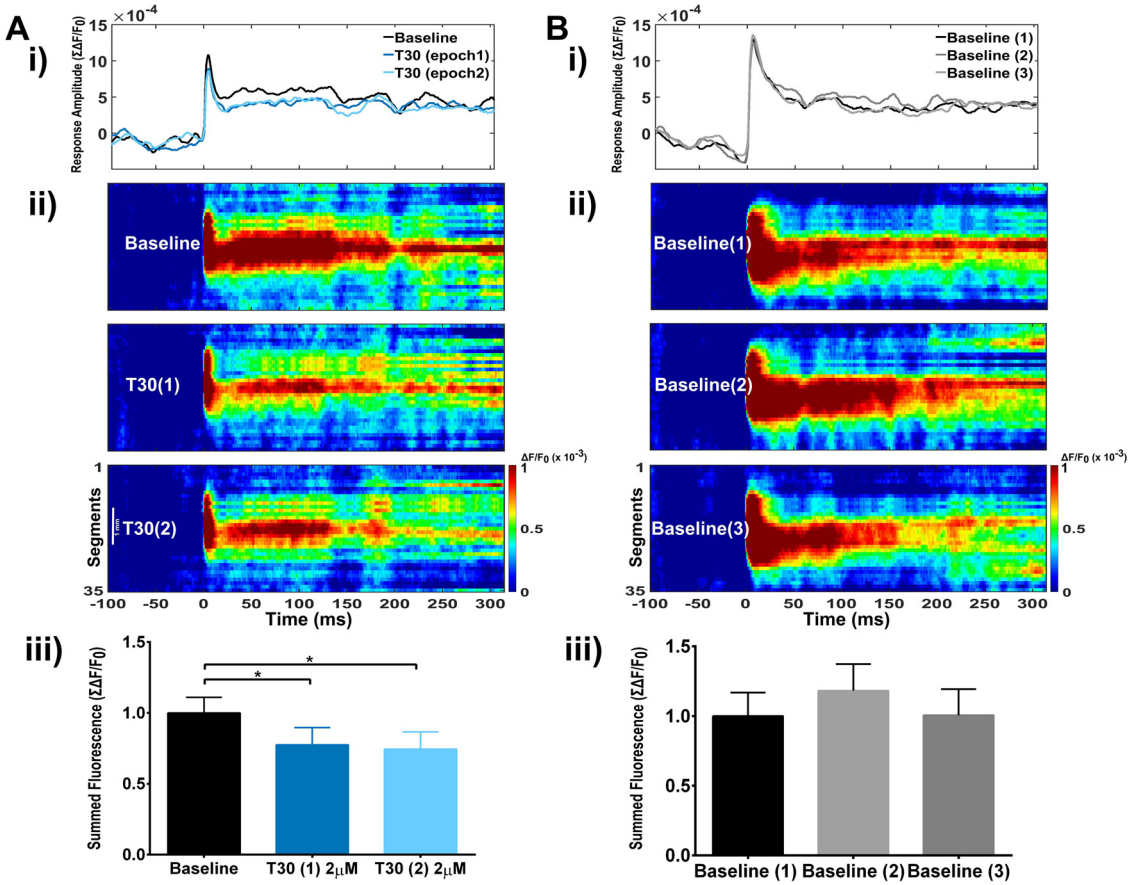

Fig. 2. T30 effects on meso-scale neuronal population activity in the BF. T30 administration (2 μM) to brain slices decreases BF-evoked activity (n = 12), compared to control recordings (n = 24) made using the same parameters (Ai-iii). Averaged time series (Ai) showing a difference in the area under the curves of baseline compared to T30 conditions, space-time maps (Aii) and bar graph of normalised summed fluorescence (Aiii) across the three treatments. Group differences: results of the Fisher LSD *post hoc* comparisons are indicated with an asterisk (*) showing differences against the baseline (Aiii). Control recordings using aCSF show no response difference between three consecutive epochs as indicated by averaged time series (Bi), space-time maps (Bii) and relative normalised bar graph (Biii). Significance levels: * $p < 0.05$; ns = non-significant. White scale bar in (Aii): 1 mm. Colour bar units: $\Delta F/F_0$.

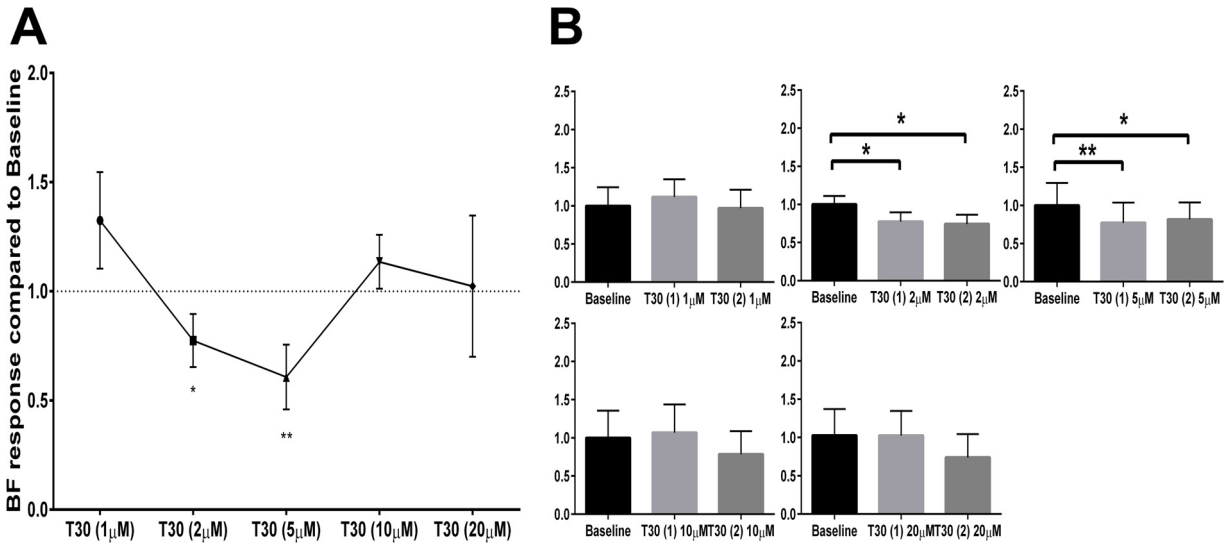

Fig. 3. Different concentrations of T30 modulate basal forebrain-evoked activity. (A) dose-response curve of T30 effects (during the first recording) on basal forebrain response normalised to baseline. While 2 (n = 12) and 5 (n = 11) μM determine a significant reduction of neuronal response compared to baseline conditions (dashed line; Baseline vs 2 μM T30(1) and Baseline vs 5 μM T30(1), unpaired *t-tests*), 1 (n = 17), 10 (n = 12) and 20 (n = 5) μM show no difference. (B) Histograms showing long-lasting effects of increasing T30 concentrations in two different recording periods. 2 and 5 μM of the peptide determine a significant decrease in activity that remains constant throughout the 2 recording epochs (group differences: results of the Fisher LSD *post hoc* comparisons are indicated with an asterisk (*) showing differences against the baseline), while with the other concentrations (1, 10 and 20 μM) the slight increase compared to baseline seen in the first recording epoch shifts to a non-significant response reduction in the second epoch. Significance levels: ** $p < 0.01$; * $p < 0.05$; ns = non-significant.

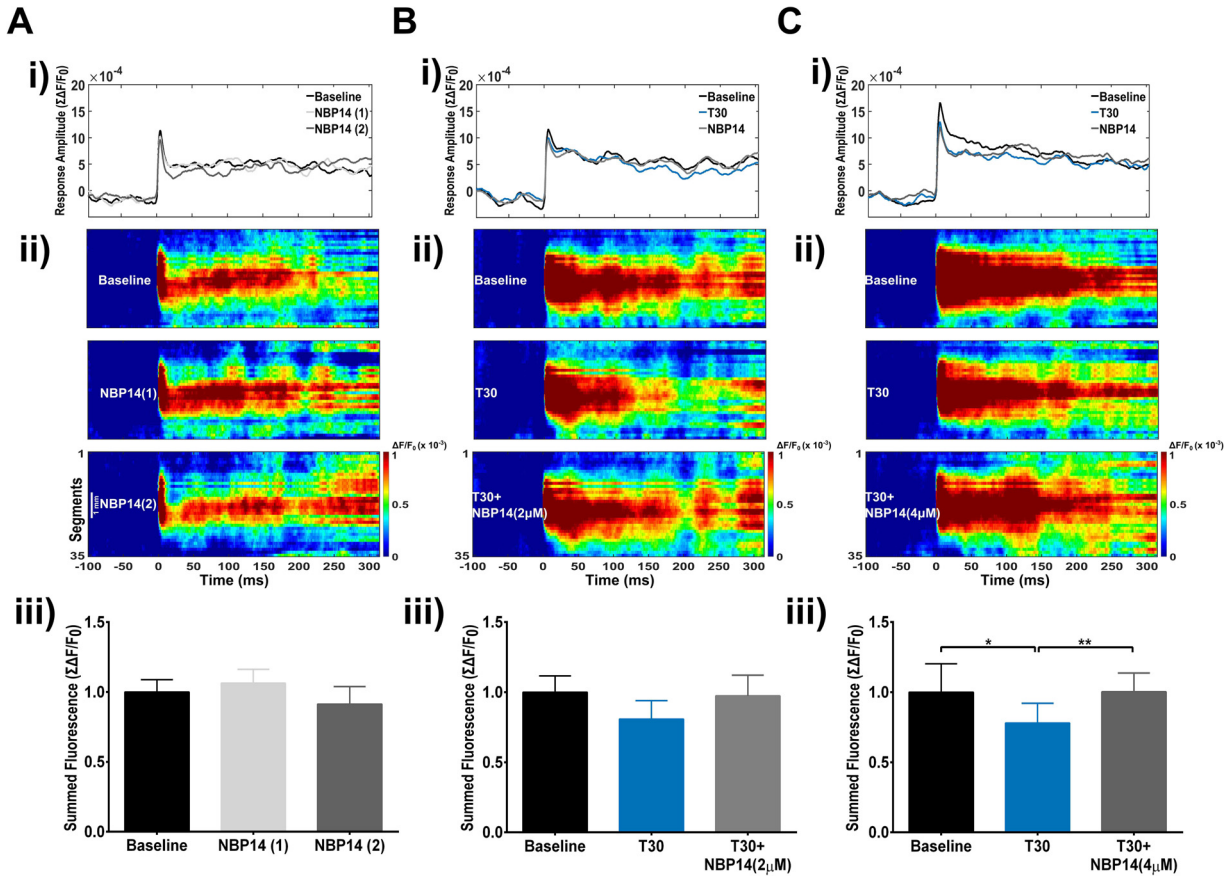

Fig. 4. Effects of NBP14 pharmacological treatment on neuronal assemblies evoked in the rat BF. (A–C): 15 min baseline recording condition (aCSF) was followed by a second recording epoch with the selected drug, either (A): NBP14(1), or (B,C): T30; and a third one with (A): NBP14(2), (B): T30 + NBP14, 2 μM or (C): T30 + NBP14, 4 μM. Each recording epoch was preceded by a 15 min period of acclimatisation to allow the habituation of the slices to the new environment. (A) NBP14 administration to the aCSF (n = 15) doesn't induce any change in the BF-evoked response as shown in the averaged time series (i), the equivalent averaged space-time maps for each recording epoch (ii) and the histogram of summed fluorescence. (B,C) VSDI time series (i), matching space-time maps (ii) and resulting bar graph of summed fluorescence (iii) evidence that in both cases T30 induces an inhibition of BF neuronal activity that is partially switched by 2 μM NBP14 application to the aCSF (n = 21), and significantly reversed by 4 μM administration of NBP14 (n = 17) confirming its dose-dependent behaviour. Group differences: results of the Fisher LSD *post hoc* comparisons are indicated with an asterisk (*) showing differences against T30. Significance levels: ** $p < 0.01$; * $p < 0.05$; ns = non-significant. White scale bar in (Aii) is 1 mm in length, colour bar units: $\Delta F/F_0$.

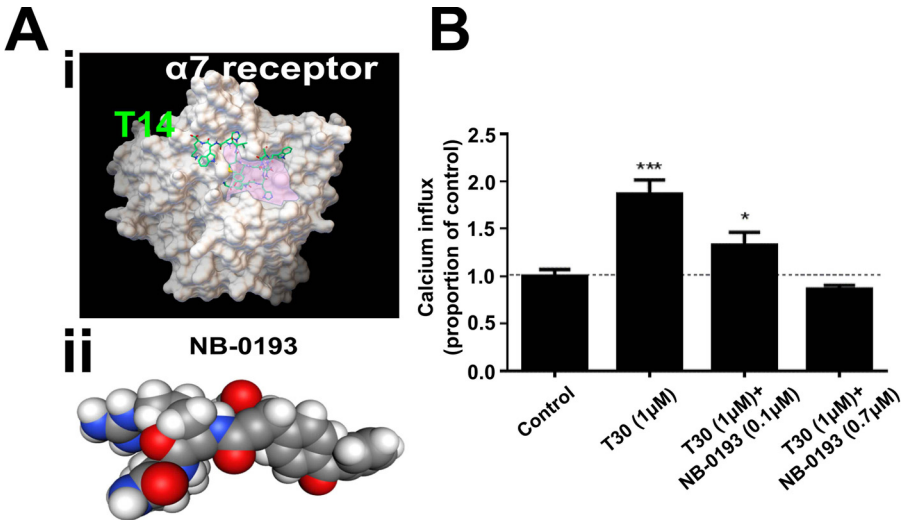

Fig. 5. Three-dimensional model of NB-0193 and its effects on PC12 cells. (Ai): Three-dimensional structure of the α7 nicotinic receptor and binding mode conformation for T14 (green), the T30 peptide's bioactive part, at the allosteric binding site (pink) obtained by docking simulations conducted with AutoDock Vina. (Aii): three-dimensional space-filling model of the molecule NB-0193, designed to exhibit a high binding affinity with the α7 nicotinic receptor to compete with T14. (B): effects of 1 μM T30 application in PC12 cells on calcium influx either alone or in the presence of NB-0193 at 0.1 or 0.7 μM in comparison to control conditions. Group differences: results of the Fisher LSD *post hoc* comparisons are indicated with an asterisk (*) showing differences against Control. Significance levels: *** $p < 0.001$; * $p < 0.05$.

properties such as stability or chemical interactions with its target α7-nACh receptor (see Methods, 2.6 and Fig. 5 Ai,ii). NB-0193 was the result of a selection of peptidomimetics with interesting features compared to NBP14 consisting in a similar aminoacidic sequence but adapted in order to make it smaller and more structurally stable (Table 1).

Table 1
Comparison between drug properties of the T14 cyclised compound NBP14 and the peptidomimetic NB-0193.

	NBP14	NB-0193
Drug properties	Cyclised peptide	Peptidomimetic
Molecular weight	1846 $gmol^{-1}$	630 $gmol^{-1}$
Binding affinity	−7.4 $kcalmol^{-1}$	−9.4 $kcalmol^{-1}$
Immunogenicity	Medium	Low

3.4. Preventative effects of NB-0193 on calcium influx in tissue culture

Previous evidence has shown the antagonistic effect of NBP14 against T30 both in *ex vivo* brain sections [29] and in cell culture [17] using three parameters that are inter-linked, a most immediate one (calcium influx) and two slightly slower (compensatory AChE release and cell viability). Before testing the new compound NB-0193 in the more physiological context of brain slices, we checked its influence on calcium entry in PC12 cells, a pheochromocytoma cell line derived from the adrenal medulla and described as a 'window' into the brain (Bornstein et al., 2012), a powerful *in vitro* model for studying neurodegenerative processes. When 1 μM T30 was administered in cell culture, it induced a strong calcium influx increment in the cells (Fig. 5 B). However, when increasing concentrations of NB-0193 were co-applied with T30, a dose-dependent preventative effect was observed, with a return to control conditions at 0.7 μM (Fig. 5 B, one way ANOVA followed by Tukey *post hoc* test, $p < 0.001$, *post hoc* comparisons: see figure). The promising results obtained in cell culture encouraged us to assess the compound in our *ex vivo* preparation.

3.5. Reversal of the effects of T30 with a peptidomimetic (NB-0193)

NB-0193 alone, like NBP14, was inert because it did not modify BF-evoked activity in brain sections by itself (Fig. 6 Ai,iii, $F_{(1.955, 27.37)} = 0.2480$, $p = 0.7772$). Space-time maps displayed a very similar activation profile of NB-0193 treated slices in comparison with the baseline (Fig. 6 Aii). We subsequently checked for dose dependency to BF stimulation using the same dilutions in aCSF as above, respectively 2 and 4 μM. Similarly to NBP14, NB-0193 when used at a lower concentration only partially alter T30 actions on BF population (Fig. 6 Bi,ii,iii, $p = 0.17$, $F_{(1.530, 44.36)} = 2.132$, $p = 0.1412$, $n = 29$). When the quantity was doubled, a significant reversal of the peptide's toxic effects was reached (Fig. 6 Ci,iii, $F_{(1.799, 34.18)} = 5.091$, $p < 0.05$, $n = 20$, *post hoc* comparisons: see figure) and this seems to be caused both by an increased network activity over space, as visible by the activation intensity on the y-axis, and over time, with a more diffused response after approximately 200 ms (Fig. 6 Cii).

3.6. Pharmacokinetic properties of NBP14 and NB-0193 in vivo

Once recognised the efficacy of NBP14 and NB-0193 in our *ex vivo* preparation, we wondered whether the compounds could show promising features also with different *in vitro* and *in vivo* approaches. As a result, we performed two different tests: first, *in vivo* pharmacokinetic studies in mice, injecting intravenously both compounds and evaluating their presence over time in different samples, blood and brain. Successively we established additional permeability studies *in vitro*.

To characterise the presence of the synthetic compounds in nude male Balb/c mouse blood and brain, *in vivo* pharmacokinetic assessment of both NBP14 and NB-0193 were conducted. NBP14 was detected in blood taken at the first three time points (2, 5, and 8 min post-dose) but was rapidly cleared and below limit of quantification (50 ng/ml) after 30 min post-dose (Fig. 7 A), while the compound was not detectable in any of the brain samples. On the other hand, NB-0193 was detected in all blood and brain samples although brain-to-blood ratios were < 0.01 (Fig. 7 B). Therefore, we decided to conduct further permeability assays in order to evaluate whether the drugs can permeate the blood-brain barrier. Specifically, the aim was to study the transcellular permeability of test compounds and the influence of P-gp-mediated efflux on drug permeability using epithelial cell line of canine kidney origin (hMDR1-MDCK) grown on filter supports (Fig. 7 C, D), with Labetolol as a positive control for P-gp activity [34–36]. This data showed extremely low permeability for NBP14, with responses close to detection limits for the receiver compartment. NB-0193 showed a relatively much higher permeability but would still be classed as a compound having low permeability (Table 2). The efflux ratios for both compounds suggest P-gp is not a factor in their low permeability.

4. Discussion

4.1. VSDI as a screening technique

The high spatiotemporal resolution of VSDI offers the opportunity for investigation and insights into large-scale neuronal networks in a wide range of brain states [37]. Moreover, of particular relevance, VSDI can also provide a powerful means for screening drugs in real-time and characterising the effects of signalling agents [37].

Techniques such as optical imaging and electrophysiology are traditionally regarded as tools of any value only in the final stages of drug discovery, due to the slow through-put [38]. Higher-throughput approaches such as cell-based assays with membrane potential or Ca^{2+} sensitive dyes or ion-flux measurements are certainly useful to identify and profile compounds but are independent of any truly physiological context [38,39]. However, such bottlenecks in the drug discovery process, could be ameliorated with the use of optical imaging as a subsequent screening after a set of primary targets has already been designated, as here.

4.2. Effects of T30 on brain slice activity

As shown previously [29] when slices are co-perfused with T30, a significant difference in response is seen, with optical imaging, when compared to control conditions.

However no change was apparent between the three recording periods using standard aCSF (see Fig. 2). These long-lasting recordings in control conditions confirmed that the decline seen after drug administration is not dependent on tissue viability of the slice, bleaching of the fluorescent dye or other artefacts.

The absence of any effect of 1 μM T30 would most likely be due to an insufficient amount of compound reaching the recording chamber, i.e. the low dose. Increasing concentrations of the peptide determined a variety of outcomes, modulating BF population response: this corresponds to the actions ranging along the trophic-toxic axis seen in different systems, as cell cultures or slices [4,17,19]. In previous studies, and indeed here cell culture studies demonstrate that increasing concentrations evoke moderately trophic effects followed by an opposite inhibitory behaviour as the concentration increases [39]. The excess of peptide can cause inhibition of calcium influx [23,39] due to phosphorylation of the channels [40] producing the depressant profile detected. Nonetheless results obtained with 2 μM, 5 μM of T30 showed a strong and significant toxic response, already attributable to calcium entry through the α7 nicotinic receptor, target of the T30 peptide [17–19,29]. This is particularly relevant during aging, where the aberrant reactivation of trophic pathways mediated by calcium and triggered by specific conditions (i.e. stroke, injuries, decline in free radical scavenging mechanisms etc.) can induce compensating responses in the form of enhanced T14 which then leads to further toxicity: hence neurodegeneration could be an inappropriate form of development [1,5,41]. Interestingly, higher concentrations revealed a different behaviour of BF meso-scale population to a stimulating protocol, more specifically they displayed a trend towards assembly

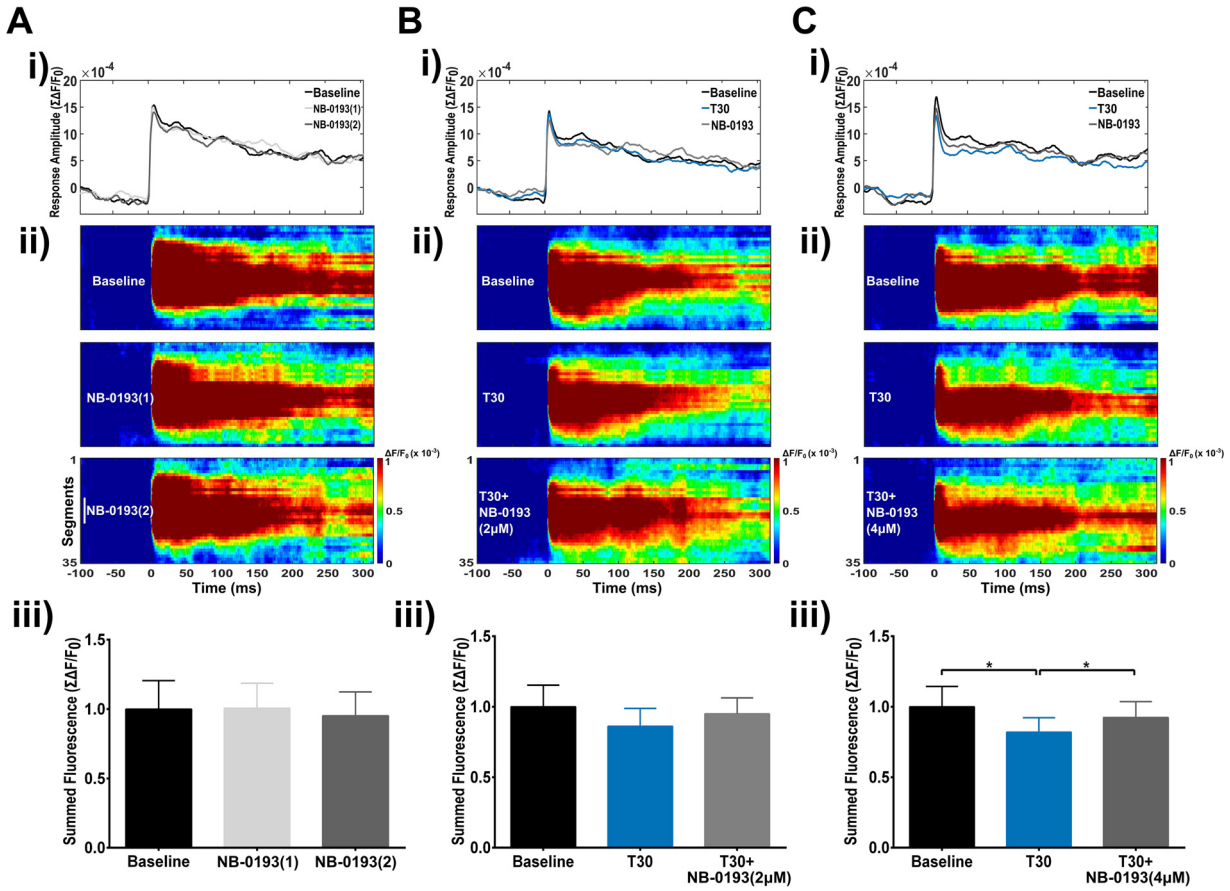

Fig. 6. Effects of the linear peptidomimetic NB-0193 on BF-evoked meso-scale activity. (A-C): 15 min baseline recording condition (aCSF perfusion) was followed by a second recording epoch with the selected drug, either (A): NB-0193(1), or (B,C): T30 and a third one with (A): NB-0193(2), (B): T30 + NB-0193, 2 μM or (C): T30 + NB-0193, 4 μM. (A) the averaged time series (i), the corresponding mean space-time maps for each recording epoch (ii) and the histogram of summed fluorescence (iii) indicate that NB-0193 administration to the aCSF (n = 15) doesn't exert any measurable change in the BF-evoked response when added to the aCSF. (B,C) VSDI time series (i) equivalent space-time maps (ii) and resulting bar graph of summed fluorescence (iii) showing T30-induced significant inhibition of BF neuronal activity that is modified by 2 μM NB-0193 application to the aCSF (n = 29), and significantly reversed by 4 μM administration of NB-0193 (n = 20) in a dose-dependent manner. Group differences: results of the Fisher LSD *post hoc* comparisons are indicated with an asterisk (*) showing differences against T30. Significance levels: * $p < 0.05$; ns = non-significant. White scale bar in (Aii) is 1 mm in length, colour bar units: $\Delta F/F_0$.

magnitude increase. Optical imaging therefore shows an inhibiting pattern at 2 and 5 μM that varies as the concentration increases, whilst cell cultures appear to respond in the reverse direction. However, this difference is most likely due to the very basic discrepancies between the two techniques. In cell culture drugs are applied for longer periods and remain in the medium at a given concentration, in VSDI, slices are surrounded by a continuous flow and the perfusion solution is constantly changing. Finally, in tissue slices, the net activity will be the result of the interplay between different neuronal networks, glia, interneurons etc., rather than a simple and direct read-out from isolated cells. In both techniques the net effect of a prolonged high dose would cause a shutting down of calcium channels [23,39] that would be seen as toxicity and eventually cell death in tissue culture and as a reduced activity with VSDI. The evoked BF population activity, regardless of the acute effect exerted by the peptide at all dilutions, unlike controls, tends to vary with time as seen during the second drug administration period (Fig. 3 B). This might be explained by the additive effect of the exogenous peptide to the high endogenous levels of the AChE-peptide already present in young animals [29]. In any event, the toxicity of AChE-peptide is reversed in PC12 cells using the cyclic compound NBP14 [17], and an analogous result was seen here in cell culture assays with NB-0193. Hence despite the diverse differences in the two techniques used, the reversal of the action of T30, whatever it may be, is comparable in these two very different preparations.

4.3. Comparison of two blockers: NBP14 and NB-0193

Neither NBP14 nor NB-0193 had any effect applied alone, testifying further to the stability of the system. However T30-induced inhibition showed a tendency towards recovery following administration of both NBP14 and also NB-0193 when applied at an equivalent low dose, and a complete and significant reversal when the concentration was doubled in each case. Moreover, the averaged time response and space time maps show that, although the peak in activation in the presence of both drugs is lower compared to baseline, the assembly size and activity after about 150 ms becomes even higher and more diffuse than in control conditions: it is possible therefore that NB-0193, similarly to NBP14 are displacing, in addition, endogenous peptide at the α7 nicotinic receptor. However, although NBP14 has previously [17,29], as here, shown promising results, its molecular weight and structure are not ideal as a possible therapeutic drug. Indeed, blood-brain barrier permeability and pharmacokinetic properties confirmed its unsuitability as a CNS (central nervous system) drug. For this reason we have used the NBP14 structure as a template for molecular modelling of a synthetic peptidomimetic NB-0193 which would have, compared to natural molecules, a higher permeability across biological barriers and a higher stability, low toxicity and negligible immunogenicity (Table 1). VSDI data demonstrates that NB-0193 shares common attributes with NBP14, but in addition NB-0193 has more attractive features in the permeability assays. This suggests that, although its permeability would be

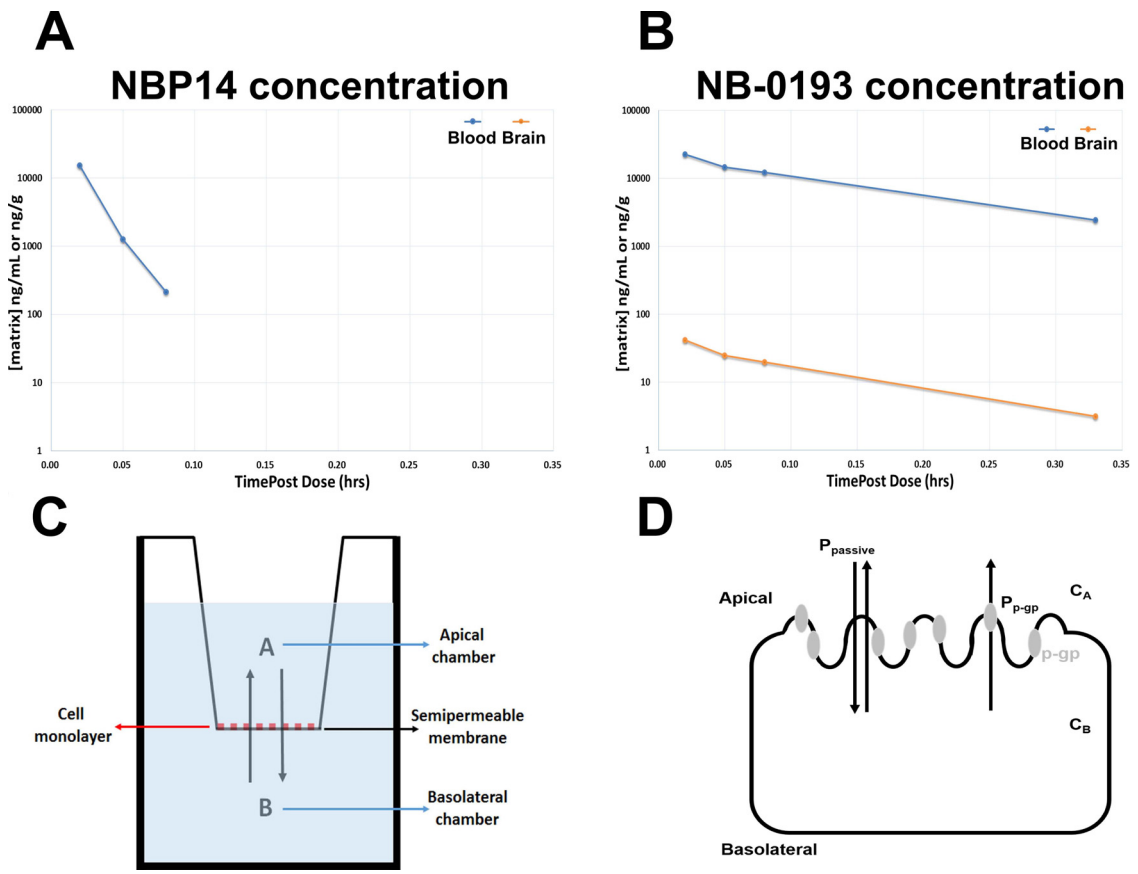

Fig. 7. NBP14 and NB-0193 stability and permeability assays: NBP14 (A) and NB-0193 (B) concentration in rat blood (blue) and brain (orange) samples calculated at different time points after the dose. (C) Experimental protocol for the study of transcellular permeability of test compounds. In this assay, the flux of a compound through a monolayer of cells (in red) grown on a porous support (in black) to separate two compartments is measured. The efflux ratio is determined by applying bidirectional measurements from apical to basolateral (A–B) and basolateral to apical (B-A). (D) Illustration of a polarised cell monolayer with permeability Glicoprotein (P-gp) actively pumping foreign substances out of cells in grey. C_a, concentration in the apical compartment; C_b, concentration in the basolateral compartment; $P_{passive}$, passive transport; $P_{P\text{-}gp}$, P-gp–mediated transport.

Table 2
Table showing the permeability, efflux ratio and properties of NBP14 and NB-0193 as P-gp substrates.

Compound	P_{app} (cm/s x 10-6)		A-B permeability	Efflux Ratio B→A/A→B
	A→B	B→A		
NBP14	0.018	0.010	Very low	0.6
NB-0193	0.21	0.24	Low	1.2
Labetolol	7.8	25.6	Medium	3.3

classed as low (Table 2), NB-0193 may have the potential for oral dosing or for use as a CNS therapeutic. Moreover, it is still possible that intranasal dosing may facilitate CNS penetration and that makes NB-0193 a good candidate for further investigation as a drug for Alzheimer's disease treatment.

5. Conclusions

In conclusion, we have demonstrated that the T30 peptide has a dose-dependent acute effect on meso-scale neuronal functioning in BF-containing rat slices. Both synthetic versions of the toxin, the cyclic peptide (NBP14) and the peptidomimetic (NB-0193), have been proven successful at blocking the consequences of excessive cellular calcium entry through the α7-nAChR in cell culture as well as in an *ex vivo* preparation. Moreover, stability and permeability assays confirmed that NB-0193 offers interesting pharmacokinetic characteristics and could therefore represent a promising therapeutic approach for arresting the neurodegenerative process typical of AD.

Author contributions

GF: responsible for all data unless otherwise noted, as well as for the preparation and writing of the manuscript. GB: responsible for data shown in Fig. 5 B. AJH: responsible for data in Fig. 7 A, B and Table 2. SG: responsible for original basic concepts, and assistance writing the manuscript.

Author information

Susan Greenfield is a Senior Research Fellow, Lincoln College Oxford. The authors declare competing financial interests. Susan Greenfield is the founder of Neuro-Bio Limited (www.neuro-bio.com), a privately owned Company, and holds shares in the Company. Giovanni Ferrati is an employee of Neuro-Bio Ltd. Georgi Bion (who has now left the company) was a full-time researcher with Neuro-Bio Ltd.

Conflict of interest

The authors declare competing financial interests: Giovanni Ferrati is currently an employee of Neuro-Bio and Georgi Bion, who has now left the company, was an employee of Neuro-Bio Ltd. Andrew Harris is an employee of the company Pharmidex (www.pharmidex.com), which provided all pharmacokinetic data for this work. Susan Greenfield is the founder and president of Neuro-Bio Ltd. and holds shares in the

company.

Acknowledgements

This project was funded by Neuro-Bio Ltd. The work described in this paper is covered by patent applications, (WO 2015/004430, GB1505239.2 and 77595GB2). We would like to thank Iproteos (www.iproteos.com) for data shown in Section 2.6 and in Fig. 5 Ai,ii. We are very grateful to Dr. Emanuele Brai and James Gould for helpful comments on the manuscript.

Appendix A. Supplementary data

Supplementary material related to this article can be found, in the online version, at doi:https://doi.org/10.1016/j.biopha.2018.10.124.

References

[1] C.A. Lane, J. Hardy, J.M. Schott, Alzheimer's disease christopher, Eur. J. Neurol. 38 (2017) 42–49, https://doi.org/10.1111/ijlh.12426.
[2] R. Katzman, The prevalence and malignancy of Alzheimer's disease, Arch. Neurol. 33 (1976) 217–218.
[3] T. Arendt, Alzheimer's disease as a loss of differentiation control in a subset of neurons that retain immature features in the adult brain, Neurobiol. Aging 21 (2000) 783–796, https://doi.org/10.1016/S0197-4580(00)00216-5.
[4] S. Greenfield, Discovering and targeting the basic mechanism of neurodegeneration: the role of peptides from the C-terminus of acetylcholinesterase: non-hydrolytic effects of ache: the actions of peptides derived from the C-terminal and their relevance to neurodegenerat, Chem. Biol. Interact. 203 (2013) 543–546, https://doi.org/10.1016/j.cbi.2013.03.015.
[5] M.N. Rossor, Parkinson's disease and Alzheimer's disease as disorders of the isodendritic core, Br. Med. J. (Clin. Res. Ed) 283 (1981) 1588–1590, https://doi.org/10.1136/bmj.284.6314.506.
[6] D.S. Auld, T.J. Kornecook, S. Bastianetto, R. Quirion, Alzheimer's disease and the basal forebrain cholinergic system: relations to β-amyloid peptides, cognition, and treatment strategies, Prog. Neurobiol. 68 (2002) 209–245, https://doi.org/10.1016/S0301-0082(02)00079-5.
[7] E.C. Ballinger, M. Ananth, D.A. Talmage, L.W. Role, Basal forebrain cholinergic circuits and signaling in cognition and cognitive decline, Neuron 91 (2016) 1199–1218, https://doi.org/10.1016/j.neuron.2016.09.006.
[8] M.M. Mesulam, The cholinergic innervation of the human cerebral cortex, Prog. Brain Res. 145 (2004) 67–78, https://doi.org/10.1016/S0079-6123(03)45004-8.
[9] N.J. Woolf, Global and serial neurons form a hierarchically arranged interface proposed to underlie memory and cognition, Neuroscience 74 (1996) 625–651, https://doi.org/10.1016/0306-4522(96)00163-7.
[10] S. Greenfield, D.J. Vaux, Commentary Parkinson' S Disease, Alzheimer' S Disease and Motor Neurone Disease : Identifying a Common Mechanism, Exp. Brain Res. 113 (2002) 485–492.
[11] M.-S. García-Ayllón, S.H. David, J. Avila, J. Sáez-Valero, Revisiting the role of acetylcholinesterase in Alzheimer's disease: cross-talk with P-tau and β-amyloid, Front. Mol. Neurosci. 4 (2011) 1–9, https://doi.org/10.3389/fnmol.2011.00022.
[12] I. Silman, J.L. Sussman, Acetylcholinesterase: 'Classical' and 'non-classical' functions and pharmacology, Curr. Opin. Pharmacol. 5 (2005) 293–302, https://doi.org/10.1016/j.coph.2005.01.014.
[13] H. Soreq, S. Seidman, Acetylcholinesterase–new roles for an old actor, Nat. Rev. Neurosci. 2 (2001) 294–302, https://doi.org/10.1038/35067589.
[14] M.S. García-Ayllón, C. Millán, C. Serra-Basante, R. Bataller, J. Sáez-Valero, Readthrough Acetylcholinesterase Is Increased in Human Liver Cirrhosis, PLoS One 7 (2012) 1–7, https://doi.org/10.1371/journal.pone.0044598.
[15] C.E. Bond, M. Zimmermann, S.A. Greenfield, Upregulation of? ?7 nicotinic receptors by acetylcholinesterase C-terminal peptides, PLoS One 4 (2009), https://doi.org/10.1371/journal.pone.0004846.
[16] M.G. Cottingham, J.L.A. Voskuil, D.J.T. Vaux, The intact human acetylcholinesterase C-terminal oligomerization domain is α-helical in situ and in isolation, but a shorter fragment forms β-sheet-rich amyloid fibrils and protofibrillar oligomers, Biochemistry 42 (2003) 10863–10873, https://doi.org/10.1021/bi034768i.
[17] S. Garcia-Ratés, P. Morrill, H. Tu, G. Pottiez, A.S. Badin, C. Tormo-Garcia, C. Heffner, C.W. Coen, S.A. Greenfield, (I) Pharmacological profiling of a novel modulator of the α7 nicotinic receptor: blockade of a toxic acetylcholinesterase-derived peptide increased in Alzheimer brains, Neuropharmacology 105 (2016) 487–499, https://doi.org/10.1016/j.neuropharm.2016.02.006.
[18] E. Brai, F. Simon, A. Cogoni, S.A. Greenfield, Modulatory effects of a novel cyclized peptide in reducing the expression of markers linked to Alzheimer's disease, Front. Neurosci. 12 (2018) 362, https://doi.org/10.3389/FNINS.2018.00362.
[19] S.A. Greenfield, T. Day, E.O. Mann, I. Bermudez, A novel peptide modulates α7 nicotinic receptor responses: implications for a possible trophic-toxic mechanism within the brain, J. Neurochem. 90 (2004) 325–331, https://doi.org/10.1111/j.1471-4159.2004.02494.x.
[20] S. Eimerl, M. Schramm, The quantity of calcium that appears to induce neuronal death, J. Neurochem. 62 (1994) 1223–1226, https://doi.org/10.1046/j.1471-4159.1994.62031223.x.
[21] T. Arendt, J. Stieler, U. Ueberham, Is sporadic Alzheimer's disease a developmental disorder? J. Neurochem. (2017) 1–13, https://doi.org/10.1111/jnc.14036.
[22] E. Brai, S. Stuart, A.-S. Badin, S.A. Greenfield, A novel ex-vivo model to investigate the underlying mechanisms in Alzheimer's disease, Front. Cell. Neurosci. 11 (2017) 291, https://doi.org/10.3389/FNCEL.2017.00291.
[23] C.L.M. Bon, S.A. Greenfield, Bioactivity of a peptide derived from acetylcholinesterase: electrophysiological characterization in guinea-pig hippocampus, Eur. J. Neurosci. 17 (2003) 1991–1995, https://doi.org/10.1046/j.1460-9568.2003.02648.x.
[24] A. Grinvald, R. Hildesheim, VSDI: a new era in functional imaging of cortical dynamics, Nat. Rev. Neurosci. 5 (2004) 874–885, https://doi.org/10.1038/nrn1536.
[25] S. Chemla, F. Chavane, Voltage-sensitive dye imaging: technique review and models, J. Physiol. Paris 104 (2010) 40–50, https://doi.org/10.1016/j.jphysparis.2009.11.009.
[26] R.D. Frostig, C.H. Chen-Bee, B.A. Johnson, N.S. Jacobs, Imaging Cajal's neuronal avalanche: how wide-field optical imaging of the point-spread advanced the understanding of neocortical structure–function relationship, Neurophoton 4 (3) (2017) 19 (2017) 031217. doi:10.1117/1.
[27] Taylor W. Schmitz, R. Nathan Spreng, The Alzheimer's Disease Neuroimaging Initiative, Basal forebrain degeneration precedes and predicts the cortical spread of Alzheimer's pathology, Nat. Commun. 7 (2016) 13249 https://doi.org/10.1038/ncomms13249.
[28] M.M. Mesulam, E.J. Mufson, A.I. Levey, B.H. Wainer, Cholinergic innervation of cortex by the basal forebrain: cytochemistry and cortical connections of the septal area, diagonal band nuclei, nucleus basalis (substantia innominata), and hypothalamus in the rhesus monkey, J. Comp. Neurol. 214 (1983) 170–197, https://doi.org/10.1002/cne.902140206.
[29] A.S. Badin, P. Morrill, I.M. Devonshire, S.A. Greenfield, (II) Physiological profiling of an endogenous peptide in the basal forebrain: age-related bioactivity and blockade with a novel modulator, Neuropharmacology 105 (2016) 47–60, https://doi.org/10.1016/j.neuropharm.2016.01.012.
[30] T.H. Grandy, S.A. Greenfield, I.M. Devonshire, An evaluation of in vivo voltage-sensitive dyes: pharmacological side effects and signal-to-noise ratios after effective removal of brain-pulsation artifacts, J. Neurophysiol. (2012) 2931–2945, https://doi.org/10.1152/jn.00512.2011.
[31] E.B. Bourgeois, B.N. Johnson, A.J. McCoy, L. Trippa, A.S. Cohen, E.D. Marsh, A toolbox for spatiotemporal analysis of voltage-sensitive dye imaging data in brain slices, PLoS One 9 (2014), https://doi.org/10.1371/journal.pone.0108686.
[32] E.P. Yu, C.G. Dengler, S.F. Frausto, M.E. Putt, C. Yue, H. Takano, D.A. Coulter, Protracted postnatal development of sparse, specific dentate granule cell activation in the mouse hippocampus, J. Neurosci. 33 (2013) 2947–2960, https://doi.org/10.1523/JNeurosci.1868-12.2013.
[33] A. Grinvald, A. Arieli, M. Tsodyks, T. Kenet, Neuronal assemblies: single cortical neurons are obedient members of a huge orchestra, Biopolymers. 68 (2003) 422–436, https://doi.org/10.1002/bip.10273.
[34] J.W. Polli, S.A. Wring, J.E. Humphreys, L. Huang, J.B. Morgan, L.O. Webster, C.S. Serabjit-Singh, Rational use of in vitro P-glycoprotein assays in drug discovery, J. Pharmacol. Exp. Ther. 299 (2001) 620–628, https://doi.org/10.1016/j.bmc.2008.09.065.
[35] S.V. Ambudkar, S. Dey, C.A. Hrycyna, M. Ramachandra, I. Pastan, M.M. Gottesman, Biochemical, cellular, and pharmacological aspects of the multidrug transporter, Ann. Rev. Pharmacol. Toxicol. 39 (1999) 361–398.
[36] B. Feng, J.B. Mills, R.E. Davidson, R.J. Mireles, J.S. Janiszewski, M.D. Troutman, S.M. De Morais, In vitro P-glycoprotein assays to predict the in vivo interactions of P-glycoprotein with drugs in the central nervous system, Drug Metab. Dispos. 36 (2008) 268–275, https://doi.org/10.1124/dmd.107.017434.
[37] S.A. Greenfield, A.-S. Badin, G. Ferrati, I.M. Devonshire, Optical imaging of the rat brain suggests a previously missing link between top-down and bottom-up nervous system function, Neurophotonics 4 (2017), https://doi.org/10.1117/1.NPh.4.3.031213 031213.
[38] J. Dunlop, M. Bowlby, R. Peri, D. Vasilyev, R. Arias, High-throughput electrophysiology: an emerging paradigm for ion-channel screening and physiology, Nat. Rev. Drug Discov. 7 (2008) 358–368, https://doi.org/10.1038/nrd2552.
[39] T. Day, S.A. Greenfield, Bioactivity of a peptide derived from acetylcholinesterase in hippocampal organotypic cultures, Exp. Brain Res. 155 (2004) 500–508, https://doi.org/10.1007/s00221-003-1757-1.
[40] T.D. Plant, N.B. Standen, Calcium current inactivation in identified neurons of helix-aspersa, J. Physiol. (Paris) 321 (1981) 273–285.
[41] G. Ferrati, E. Brai, S. Stuart, C. Marino, S. Greenfield, A multidisciplinary approach reveals an age-dependent expression of a novel bioactive peptide, already involved in neurodegeneration, in the postnatal rat forebrain, Brain Sci. 8 (2018) 132, https://doi.org/10.3390/brainsci8070132.
[42] G. Paxinos, C. Watson, The Rat Brain in Stereotaxic Coordinates, Acad. Press, 1998.